Benzene under ultrashort XUV laser fields: a time-dependent density functional study

Bachelorarbeit

zur Erlangung des akademischen Grades eines
Bachelor of Science

an der Karl-Franzens-Universität Graz

vorgelegt von
Siegfried Kaidisch

am Institut für Theoretische Physik
Betreuer: Assoz.-Prof. Dr. Peter Puschnig

Graz, 2019

Abstract

As pump-probe photoemission experiments are a key element of understanding short-timescale electronic behaviour, their modelling and ab-initio description is of special interest.
This thesis serves as a first step for the FWF-project "Photoemission Tomography of Excited Molecular States" which is a joint project between the Institute of Physics, KFU Graz (Georg Koller, Peter Puschnig) and the group for ultrafast XUV (extreme ultraviolet) laser physics at the University of Nova Gorica, Slovenia (Giovanni de Ninno) which will focus on the description of pump-probe photoemission experiments.
In the present work calculations are performed in the OCTOPUS-code, a real-space density functional code. The aim of this work is to get a better understanding of the default absorbing boundary used in the OCTOPUS-code as well as to gain first results for benzene's behavior under an ultrashort, strong XUV laser pulse.

Contents

1 Introduction

Density functional theory (DFT) and its time-dependent form (TDDFT) are widely used frameworks for investigating properties of many-electron systems. Their major advantage - in contrast to solving the many-body Schrödinger equation (MBSE) - is the decrease in numerical complexity, thanks to them being effective one-body formalisms. While theoretically both DFT (due to the Hohenberg-Kohn theorem) and TDDFT (due to the Runge-Gross theorem) are exact, meaning the resulting equations contain the same information as the MBSE, in reality approximations have to be made, not only because of computational concerns but especially because they contain the so called exchange-correlation functional, whose exact form is not known.

When performing numerical calculations of molecules interacting with external laser fields, a simulation box containing the molecule is employed and by defining a space grid numerical calculations can be executed on the discrete gridpoints. If now the interest lies in ionization simulations a fundamental problem arises from this setup: Electrons leave the molecule and approach the boundary of the simulation box. In order to prevent the electrons from being reflected, which would be an unphysical behaviour, absorbing boundaries need to be employed. Even though no absorbing boundary (AB) with perfect absorption, i.e. zero reflection can exist ([1], p.632), approaches like the mask-function (MF) or complex absorbing potentials (CAP) deliver satisfying results. An important parameter for the success of both theories is the width of the AB region. In the first part of this work the influence of the ABs width on the absorption quality is analyzed for a MF AB.

Moreover, the behavior of benzene under ultrashort (few-femtosecond), strong XUV (10 eV) laser fields is studied. By varying the laser's intensity, the dependency of the number of photoelectrons on the intensity is studied.

In Section 2 the theoretical background of DFT and TDDFT is given, as well as the basic idea of MF and CAP ABs. In Section 3 the performed simulations (Calculations are performed in the DFT OCTOPUS-code) are described, while in Section 4 the results are presented. In Section 5 a short discussion of the results is presented, while Section 6 summarizes the results.

2 Theoretical Foundation

This work uses a non-relativistic, quantum-mechanical approach in describing the valence-electrons' motion. Inner electrons are taken into account by a pseudopotential. Nuclei are treated in the Born-Oppenheimer approximation. Laser fields are treated classically.
In this chapter, first, DFT and TDDFT fundamentals are described, followed by an introduction to ABs.

2.1 Molecular Schrödinger Equation

This chapter is based on [2].
The (time-independent) many-body Schrödinger equation (MBSE) of a system of N electrons and K nuclei constists of five parts: The kinetic energy of the electrons, the Coulomb interaction between the electrons, the Coulomb interaction between nuclei and electrons, the kinetic energy of the nuclei and the Coulomb interaction between the nuclei.

$$\hat{H} = -\frac{1}{2}\sum_{i=1}^{N}\Delta_i + \frac{1}{2}\sum_{i,j\neq i}\frac{1}{|\boldsymbol{r}_i - \boldsymbol{r}_j|} - \sum_{i=1}^{N}\sum_{k=1}^{K}\frac{Z_k}{|\boldsymbol{r}_i - \boldsymbol{R}_k|} - \frac{1}{2M_k}\sum_{k=1}^{K}\Delta_k + \frac{1}{2}\sum_{k,l\neq k}\frac{Z_k Z_l}{|\boldsymbol{R}_k - \boldsymbol{R}_l|} \tag{1}$$

$$\hat{H}\psi\left(\{\boldsymbol{r}_i\},\{\boldsymbol{R}_k\}\right) = E\psi\left(\{\boldsymbol{r}_i\},\{\boldsymbol{R}_k\}\right) \tag{2}$$

In the Born-Oppenheimer approximation the coordinates of the nuclei are taken to be fixed, which is a good approximation in processes on a timescale of electronic movements, since the nuclei, due to their much bigger masses, are more inert than the eletrons and therefore hardly move during such processes (seen from the atoms frame of reference). Applying the Born-Oppenheimer approximation to the MBSE the kinetic energy term of the nuclei vanishes and the Coulomb interaction term between the nuclei becomes a constant C and may be substracted from the total energy term in the MBSE. The MBSE takes the form:

$$\hat{H}_{BO} = -\frac{1}{2}\sum_{i=1}^{N}\Delta_i + \frac{1}{2}\sum_{i,j\neq i}\frac{1}{|\boldsymbol{r}_i - \boldsymbol{r}_j|} + -\sum_{k=1}^{K}\frac{Z_k}{|\boldsymbol{r} - \boldsymbol{R}_k|}) \tag{3}$$

$$\hat{H}_{BO}\psi\left(\{\boldsymbol{r}_i\}\right) = (E - C)\,\psi\left(\{\boldsymbol{r}_i\}\right) \tag{4}$$

An additional appoximation that is often applied is to neglect the complex motion of the inner electrons (as they often are not of interest e.g. in chemical bonding processes) by including their effect on valence electrons only by an additional effective potential, a so called pseudopotential. This approximation is also applied in the current work.
Although the Born-Oppenheimer approximation makes numerical calculations easier, further approximations have to be made for larger systems.

2.2 DFT (KS-DFT)

First of all, it is important to mention that the following formalism is in principle no approximation but exact. Nevertheless, as will be mentioned later on, approximations are inevitable.
As one could guess the electronic density plays a fundamental role in DFT. In the following its role in the Kohn-Sham formalism is outlined. The basic idea of Kohn and Sham was to introduce an auxilary (imaginary) system of so called Kohn-Sham electrons (KS-electrons) which behave just like normal electrons with only one difference: The KS-electrons do not interact with each other. To compensate for the neglected interaction additional potentials are introduced in the Schrödinger equation.

$$\left(-\frac{1}{2}\nabla^2 + v_{\text{ext}}(\mathbf{r}) + v(\mathbf{r}) + u(n;\mathbf{r}) + v_{\text{xc}}\left(n;\mathbf{r}\right)\right)\psi_{\alpha\sigma}(\mathbf{r}) = \varepsilon_{\alpha\sigma}\psi_{\alpha\sigma}(\mathbf{r}) \tag{5}$$

The KS-electron-nucleus interaction is given by

$$v(\mathbf{r}) = -\sum_{k=1}^{K}\frac{Z_k}{|\boldsymbol{r} - \boldsymbol{R}_k|} \tag{6}$$

The Coulomb interaction of the real electrons is included by the Hartree potential (functional)

$$u(n;\mathbf{r}) = \int \mathrm{d}^3r'\frac{n\left(\mathbf{r}'\right)}{|\mathbf{r} - \mathbf{r}'|} \tag{7}$$

In (5) an external, constant (in time) potential v_{ext} was added, which is just a sum of all external potentials.
The exchange-correlation potential (xc functional) $v_{\mathrm{xc}}(n;\mathbf{r})$ should ideally contain all up to now neglected many-electron phenomena. However, at this point approximations are to be made, because its exact form is not known. Before taking a look at the xc potential approximation the idea of KS-DFT shall be concluded.
From the KS-wavefunctions $\psi_{\alpha\sigma}(\mathbf{r})$ the (spin-independent) electron density can be calculated by summing over all occupied states and both spin possibilities:

$$n(\mathbf{r}) = \sum_{\sigma} \sum_{\alpha}^{occ} |\psi_{\alpha\sigma}(\mathbf{r})|^2 \tag{8}$$

(5) and (8) are solved iteratively, i.e. starting from an initial guess of n (in our case a LCAO ansatz) the equations are solved upon self-consistency is achieved. The vital point is now, that by virtue of the Hohenberg-Kohn theorem, every ground state property of the system is a functional of the density (albeit the functional form might not be known), i.e. the density includes all information of the ground state, just like the many-body wavefunction does (Furthermore, if the exact form of the xc functional was used for calculating the KS wavefunctions, the "KS-density" calculated from (8) would be exactly the same density, as the real electrons' one.). This means that all the numerical MBSE difficulties are transfered into the form of the xc functional. Thus, by a good approximation of the xc functional, ground state properties can be calculated using the KS formalism, as long as the density functional (a functional which is dependent on the density) of the property of interest is known. Later on in chapter 3.2 DFT, as it is a ground state theory, will be used to calculate the ground state KS-wavefunctions (GS-KS-wavefunctions) of benzene, which will be used later on in time-dependent calculations.

XC Functionals

As mentioned before, the challenge in DFT - as well as in TDDFT - is to find a suitable approximation of the xc functional. Below, three types of xc potentials are presented.

- LDA: In the "local density approximation" the xc functional is a functional, solely dependent on the density. Its local contribution is approximated by the properties of a homogeneous electron-gas.
- GGA: In a "Generalized gradient approximation" the functional is taken to be dependent not only on the density, but also on its spatial derivate.
- MGGA: A "Meta-GGA" functional is furthermore also dependent on the density's Laplacian.

In the present work an LDA is used, since an LDA calculation is generally faster than a GGA (or MGGA) calculation.
For a more detailed introduction on DFT one may refer to [3], which this section is also based on.

2.3 TDDFT

Dealing with time-dependent problems, the time-dependent version of (5) determines the evolution of the system

$$\left(-\frac{1}{2}\nabla^2 + v_{\text{ext}}(\mathbf{r},t) + v(\mathbf{r},t) + u(n;\mathbf{r},t) + v_{\text{xc}}\left(n;\mathbf{r},t\right)\right)\psi_{\alpha\sigma}(\mathbf{r},t) = i\frac{\partial}{\partial t}\psi_{\alpha\sigma}(\mathbf{r},t) \tag{9}$$

with a time-dependent external potential $v_{\text{ext}}(\mathbf{r},t)$ e.g. a laser pulse.
The nucleus-electron-interaction potential is implicitly time-dependent, because of the time-dependence of $\mathbf{r}$ (again in the Born-Oppenheimer approximation).
The time-dependent Hartree potential is given by

$$u(n;\mathbf{r},t) = \int \mathrm{d}^3r' \frac{n\left(\mathbf{r}',t\right)}{|\mathbf{r}-\mathbf{r}'|} \tag{10}$$

The time-dependency of the xc potential can be introduced by different approaches, one of which is the adiabatic approximation, which includes time-dependence in the following manner

$$v_{\text{xc}}^{\text{adiabatic}}\left(\boldsymbol{r},t\right) = v_{\text{xc}}\left(n;\boldsymbol{r}\right)\big|_{n=n(t)} \tag{11}$$

From the resulting KS-wavefunctions, again, the density can be calculated by

$$n(\mathbf{r},t) = \sum_{\sigma} \sum_{\alpha}^{occ} |\psi_{\alpha\sigma}(\mathbf{r},t)|^2 \tag{12}$$

Using the GS-KS-wavefunctions as initial states, (9) and (12) determine the system's time-evolution.
The key to success in TDDFT is - just like the Hohenberg-Kohn theorem in DFT - the Runge-Gross theorem. It states, that the density (12) contains the same information, as the time-dependent many-body wavefunction and that every property of the system is a functional of the density.
Above descriptions and further information on TDDFT can be taken from [4]

2.4 Absorbing Boundaries

Equipped with DFT and TDDFT one can now try and study the behavior of molecules under strong laser pulses, leading to ionization. When doing simulations of such a process a simulation box is created which contains the molecule. Ionization leads to the electrons reaching the outer boundaries of the box. To prevent the unphysical behaviour of reflections of the electrons at the boarder, absorbing boundaries can be employed. Depending on their properties, e.g. their width, the amount of reflected density can be minimalized. In the following, two different types of ABs are presented.

Mask-Function ABs

The basic idea of mask-function (MF) ABs, as presented in [5] p.4 ff., is the following:
From now on, the area of interest, i.e. the simulation box will be refered to as region A. Directly connected to A, at its outer boundary, a new region, called B is installed (However, B will not appear in the technical realisation of the MF AB). Furthermore, the very outer shell of A, will be called region C, will operate as a connection between A and B and will act as the absorbing boundary.
The first step is to split the KS-wavefunctions into two parts

$$\psi_i(\mathbf{r},t) = \psi_{A,i}(\mathbf{r},t) + \psi_{B,i}(\mathbf{r},t) \tag{13}$$

At this point the mask-function $0 < M(\mathbf{r}) < 1$ is introduced, defining how the partial wavefunctions are calculated from the original ones

$$\psi_{A,i}(\mathbf{r},t) = M(\mathbf{r})\psi_i(\mathbf{r},t) \tag{14}$$

$$\psi_{B,i}(\mathbf{r},t) = [1 - M(\mathbf{r})]\psi_i(\mathbf{r},t) \tag{15}$$

The time-evolution is then done in a similar manner:

$$\psi_{A,i}(\mathbf{r},t') = M(\mathbf{r})U(t',t)\left[\psi_{A,i}(\mathbf{r},t) + \psi_{B,i}(\mathbf{r},t)\right] \tag{16}$$

$$\psi_{B,i}(\mathbf{r},t') = [1 - M(\mathbf{r})]U(t',t)\left[\psi_{A,i}(\mathbf{r},t) + \psi_{B,i}(\mathbf{r},t)\right] \tag{17}$$

The trick is now to define $M(\mathbf{r})$ in a way that it is 1 in the inner region of A (A without C), 0 in B and a smooth transition from 1 to 0 in C (typically by a $\sin^2$ function). Thus $\psi_{A,i}(\mathbf{r},t')$ describes states in region A and $\psi_{B,i}(\mathbf{r},t')$ describes states in B, while in C the two wavefunctions overlap, allowing movement from one region to another

Assuming the photoelectrons in region B not to interact with each other and to evolve as free particles, their movement (in the external field) is analytically solvable and described by non-interacting *Volkov states* with a time-propagator (vector potential $\mathbf{A}(\tau)$)

$$U_V(t',t) = \exp\left\{-i\int_t^{t'} \mathrm{d}\tau \frac{1}{2}\left[\mathbf{p} - \frac{\mathbf{A}(\tau)}{c}\right]^2\right\} \tag{18}$$

Thus, the idea is to modify (16) and (17) in a way that the evolution in A is calculated numerically from the Schrödinger equation, while in B, the free movement is calculated analytically with C - as stated above - serving as a bridge between A and B.

In PES calculations $\psi_{B,i}(\mathbf{r},t')$ is of interest. In our case, as our focus lies in the absorbing behaviour of the mask function, $\psi_{A,i}(\mathbf{r},t')$ is of interest.

As stated above, the OCTOPUS simulation box corresponds to region A, with its very outer shell C acting as the absorbing boundary. Thus, the time evolution in the simulation box is given by

$$\psi_{A,i}(\mathbf{r},t') = \eta_{A,i}(\mathbf{r},t') + \eta_{B,i}(\mathbf{r},t'), \tag{19}$$

with

$$\eta_{A,i}(\mathbf{r},t') = M(\mathbf{r})U(t',t)\,\psi_{A,i}(\mathbf{r},t) \tag{20}$$

evolving the wavefunction localized in A and

$$\eta_{B,i}(\mathbf{r},t') = M(\mathbf{r})\int \frac{\mathrm{d}\mathbf{p}e^{i\mathbf{p}\cdot\mathbf{r}}}{(2\pi)^{\frac{d}{2}}}U_V(t',t)\,\tilde{\psi}_{B,i}(\mathbf{p},t) \tag{21}$$

taking electrons moving back from B to A into account.
Thus the mask-function $M(\mathbf{r})$ multiplies the density in C by a factor smaller than one, i.e. acts as an AB.
In [5] an evolution of $\psi_{A,i}(\mathbf{r},t')$ according to (19) is referred to as the "full mask method", while in the reduced mask method, which is then just referred to as the "mask method" electrons moving from B to A are neglected (thus $\eta_{B,i}(\mathbf{r},t') = 0$). In this sense, the present work uses a mask function AB which is also the default OCTOPUS option (input variable *PESMaskMode*, [6]).

Complex Absorbing Potential ABs

The idea of complex absorbing potential (CAP) ABs is to modify the outer shell C of the simulation box A (just like the regions were named before for the MF AB), by applying a new potential $V_{\mathrm{CAP}}(x)$. Extended to the whole space, $V_{\mathrm{CAP}}(x)$ is taken to be 0 deep inside of A (inner sphere, i.e. A without C) and a negative, complex potential in region C. Thus, the time-evolution operator becomes the following

$$U_{CAP}(t+\Delta t,t) = e^{-iH\Delta t} = e^{-i[H_0+V_{\mathrm{CAP}}(x)]\Delta t}, \tag{22}$$

where the Hamiltonian H_0 is defined by (9). In the inner sphere of region A, U_{CAP} reduces to $e^{-iH_0\Delta t}$, while in region C it becomes non-unitary and because of the complex potential $V_{\mathrm{CAP}}(x)$ being chosen to be negative, an exponential damping is employed.
The CAP AB's depth has to be adapted to the problem of interest. For the present work the MF AB thus turned out to be the more convenient choice. For more detailed information on CAPs one may refer to [7] p.6 f. where it is also shown that CAP and MF ABs can formally be transformed into each other (p.7 f.).

A Remark on Units

Throughout most of this work, a modified version of the atomic system of units will be used, i.e. starting from the basic definitions of atomic units the unit of length is set to be Angstrom and the unit of energy to eV. This leads to eV^{-1} being the unit of time with

$$eV^{-1} \approx 6.58210^{-16}\ s \tag{23}$$

Later on, laser intensities will be presented in W/cm^2. The relation between the intensity I and the amplitude E of the electric field is given by

$$I = \frac{c}{8\pi} E^2 \tag{24}$$

Given the field amplitude E in the used system of units ($[E] = \frac{eV}{\text{Å}}$) the value of I is given by

$$I = 1.327 \times 10^{13} \left(E^2\right) \text{W/cm}^2 \tag{25}$$

This will be useful as the OCTOPUS-code does not take I but rather E to define the electric field.
An introduction to units in OCTOPUS can be found in [8].

3 Simulations

This section gives a summary of the simulations performed in the OCTOPUS-code (Version 8.3) outlining the behaviour of benzene under an ultrashort (few-femtosecond) laser pulse: The aim is to calculate the dependency of the number of photoelectrons (later plots will show the number of electrons *remaining* in the simulation box) on the lasers intensity. The simulation was done in the following order: First of all, starting from an initial guess, a geometry optimization for the benzene molecule was performed. Next, a ground state calculation had to be done, in order to receive the GS-KS-wavefunctions, which served as a starting point for the time-dependent calculations. Afterwards, the behaviour of the molecule was compared for different widths of the absorbing boundary (MF AB). After having found a sufficient AB-width, in the last step the number of emitted electrons was calculated for different laser intensities.

3.1 Geometry Optimization

As a first guess, the binding angles between the atoms were set to be $\alpha = 120°$. The bond length between the carbon atoms was guessed to be $cc = 1.4$ Å, the one between carbon and hydrogen as $ch = 1.1$ Å.
Using the following input file the geometry was calculated:

```
CalculationMode = go

FromScratch = yes
UnitsOutput = eV_Angstrom



cc    = 1.4*angstrom
ch    = 1.1*angstrom
alpha = 120
phi   = (alpha-90)*pi/180
%Coordinates
  "C" |                  0 |       cc*(0.5 +sin(phi)) |      0
  "C" |       cc*cos(phi) |                   cc*0.5 |      0
  "C" |       cc*cos(phi) |                  -cc*0.5 |      0
  "C" |                  0 |      -cc*(0.5 +sin(phi)) |      0
```

```
  "C" |      -cc*cos(phi) |                  -cc*0.5 |      0
  "C" |      -cc*cos(phi) |                   cc*0.5 |      0
  "H" |                  0 |    cc*(0.5 +sin(phi))+ch |      0
  "H" |  (cc+ch)*cos(phi) |       cc*0.5+ch*sin(phi) |      0
  "H" |  (cc+ch)*cos(phi) |    -(cc*0.5+ch*sin(phi)) |      0
  "H" |                  0 | -(cc*(0.5 +sin(phi))+ch) |      0
  "H" | -(cc+ch)*cos(phi) |    -(cc*0.5+ch*sin(phi)) |      0
  "H" | -(cc+ch)*cos(phi) |     (cc*0.5+ch*sin(phi)) |      0
%

BoxShape = sphere
Radius   = 5*angstrom
Spacing  = 0.18*angstrom
```

Once a convergence criterion (in this case the default criterion "$GOTolerance = 0.051\ eV/$Å", which sets an upper boundary for the combined forces on each atom) is achieved, a file "min.xyz" is created, containing the converged atomic positions:

```
 12
units: A
     C                  -0.000000    1.386693    0.000000
     C                   1.200720    0.693275    0.000000
     C                   1.200720   -0.693275    0.000000
     C                   0.000000   -1.386693    0.000000
     C                  -1.200720   -0.693275    0.000000
     C                  -1.200720    0.693275    0.000000
     H                  -0.000000    2.479164    0.000000
     H                   2.146810    1.239498    0.000000
     H                   2.146810   -1.239498    0.000000
     H                  -0.000000   -2.479164    0.000000
     H                  -2.146810   -1.239498    0.000000
     H                  -2.146810    1.239498    0.000000
```

This file has been used in all upcoming calculations.

3.2 Ground State Calculation

First of all it is important to mention that the box parameters (radius, spacing) of the ground state calculation needed to be the same as later on in the time-dependent runs, because the GS-KS-wavefunctions calculated in this step are bound to them. Having that said, the simulation parameters will be outlined next:
The (spherical) simulation box consists of two regions: An inner sphere, where the density evolves according to (9) and (12) and an outer shell (previously named as region C) which acts as the absorbing boundary. This inner sphere was chosen to have a radius of 10 Å, in order not to cut off any bound electronic states. The outer shell's width was varied from 0.1 Å to 5 Å.
The spacing was obtained by trying out various settings and choosing a tradeoff between calculation-time and accuracy.
An input file (in this case for the use with a 0.1 Å AB) is shown below.

```
CalculationMode = gs

UnitsOutput = eV_Angstrom

XYZCoordinates = 'min.xyz'

BoxShape = sphere
Radius   = 10.1*angstrom
Spacing  = 0.18*angstrom

Output         = density
OutputFormat   = cube + plane_z

ConvEigenError       = true
EigensolverTolerance = 1e-6
MaximumIter          = 1000
```

Starting from an LCAO ansatz an iterative DFT calculation is done, which in this case ends with a convergence criterion for the relative change in the eigenvectors *EigensolverTolerance = 1e-6* from one step to another.

Even though for most radii after 1000 iterations the criterion was not met (mostly all but one eigenvectors fullfilled the criterion), the resulting set of eigenvectors was converged well enough for further calculations (they all fullfilled *EigensolverTolerance = 1e-5*). Once the calculation is finished, a directory "restart/gs" is created, containing the required files for the time-dependent calculations.
This calculation was repeated for different radii from 10.1 Å to 15 Å, corresponding to AB-widths from 0.1 Å to 5 Å in order to obtain the GS-KS wavefunctions for the time-dependent calculations.

3.3 Time-Dependent Runs

For the time-dependent runs a time step small enough to keep the calculation numerically stable, but large enough to keep computational time low, must be established. To find an appropriate time-step, runs without an external perturbation were performed, lowering the timestep, until the total energy of the molecule was conserved during these calculations. The propagation time was chosen to be large enough to have the photoelectrons reach the simulation box boundary and be absorbed, while the time propagation itself was done by the classical Crank-Nicolson-propagator.
The perturbation is given by an ultrashort laser pulse described by a Gaussian envelope function centered in time around 3 eV^{-1}, which is definetly "late enough", to not cut off a relevant part of the beginning of the Gaussian curve and a standard deviation of 0.76 eV^{-1} (in seconds: $\sim 0.5\ fs$ standard deviation, $\sim 1.18\ fs$ FWHM). The laser's energy was chosen to be 10 eV with a polarization along the first direction. The electric field amplitude is varied during the calculations.
A plot of the laser (in this case with an intensity $I = 10^{16}\ \frac{W}{cm^2}$) is shown in Figure 1.

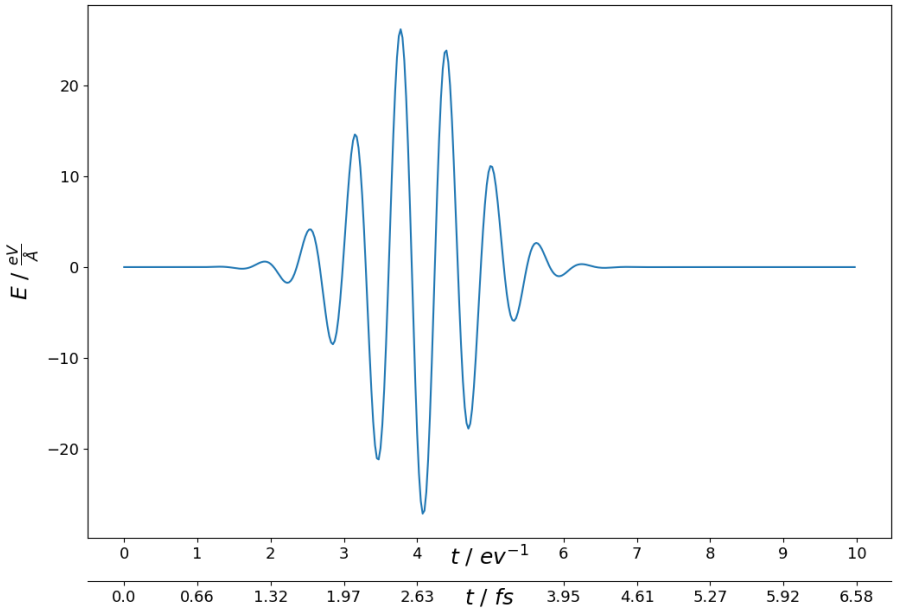

Figure 1: Electric Field amplitude of the $10^{16}\ \frac{W}{cm^2}$ laser pulse

3.3.1 Finding a Sufficient AB-Width

The aim of the first part of the time-dependent calculations was to compare the number of emitted electrons for different AB-widths (0.1 Å, 0.25 Å, 0.5 Å, 0.75 Å, 1 Å, 2 Å, 3 Å, 4 Å, 5 Å) of a MF AB (leaving the shape of the mask-function at its default $\sin^2$ form, input variable *PESMaskShape*, [6]). In these calculations a laser intensity of about $10^{17}\ W/cm^2$ was used.
The following shows the input file for the calculation with a 2 Å AB.

```
CalculationMode = td

UnitsOutput = eV_Angstrom

XYZCoordinates = 'min.xyz'
```

```
BoxShape = sphere
Radius   = 12*angstrom
Spacing  = 0.18*angstrom

TDTimeStep        = 0.025/eV
TDPropagationTime = 15/eV
TDPropagator      = crank_nicolson

#Laser Field
amplitude = 86.81*eV/angstrom    #E
omega     = 10*eV
tau0      = 0.76/eV
t0        = 3/eV

%TDExternalFields
  electric_field | 1 | 0 | 0 | omega | "envelope_gaussian"
%

%TDFunctions
  "envelope_gaussian" | tdf_gaussian | amplitude | tau0 | t0
%

#Absorbing boundary
AbsorbingBoundaries = mask
%ABShape
   10*angstrom | 12*angstrom
%

#Output
TDOutput       = laser + multipoles + energy
OutputInterval = 10
Output         = density
OutputFormat   = cube + plane_z
```

The results are presented in Section 4.2.

3.3.2 Intensity Dependence of the Number of Valence Electrons

The second part of the time-dependent calculation used an AB-width of 2 Å, which turned out to be sufficient from the calculations above (see Section 4.2). As laser intensities the following values were used: 10^{13} W/cm^2, 10^{14} W/cm^2, 10^{15} W/cm^2, 10^{16} W/cm^2, 10^{17} W/cm^2 varying the parameter *amplitude* in the following input file (here it is set to be 10^{17} W/cm^2).

```
CalculationMode = td

UnitsOutput = eV_Angstrom

XYZCoordinates = 'min.xyz'

BoxShape = sphere
Radius   = 12*angstrom
Spacing  = 0.18*angstrom

TDTimeStep        = 0.025/eV
TDPropagationTime = 100/eV
TDPropagator      = crank_nicolson

#Laser Field
amplitude = 86.81*eV/angstrom    #E
omega     = 10*eV
tau0      = 0.76/eV
t0        = 3/eV

%TDExternalFields
  electric_field | 1 | 0 | 0 | omega | "envelope_gaussian"
%

%TDFunctions
  "envelope_gaussian" | tdf_gaussian | amplitude | tau0 | t0
%

#Absorbing boundary
AbsorbingBoundaries = mask
```

```
%ABShape
   10*angstrom | 12*angstrom
%

#Output
TDOutput       = laser + multipoles + energy
OutputInterval = 10
Output         = density
OutputFormat   = cube + plane_z
```

In chapter 4.3 the results for the different intensities are presented

4 Results

4.1 Kohn-Sham Energies

As they may be of interest, in this section the energies of the Kohn-Sham electrons obtained in Section 3.2 are presented (while keeping in mind that these energies in general will not coincide with the real electrons' energy eigenvalues):

Table 1: KS energies (rounded to two digits) of benzene (each state is occupied twice)

#	energy / eV
1	−6.57
2	−6.57
3	−8.29
4	−8.29
5	−9.36
6	−10.32
7	−10.32
8	−11.02
9	−11.20
10	−13.05
11	−14.83
12	−14.83
13	−18.40
14	−18.40
15	−21.29

The corresponding density distribution in the z=0-plane is shown in Figure 2

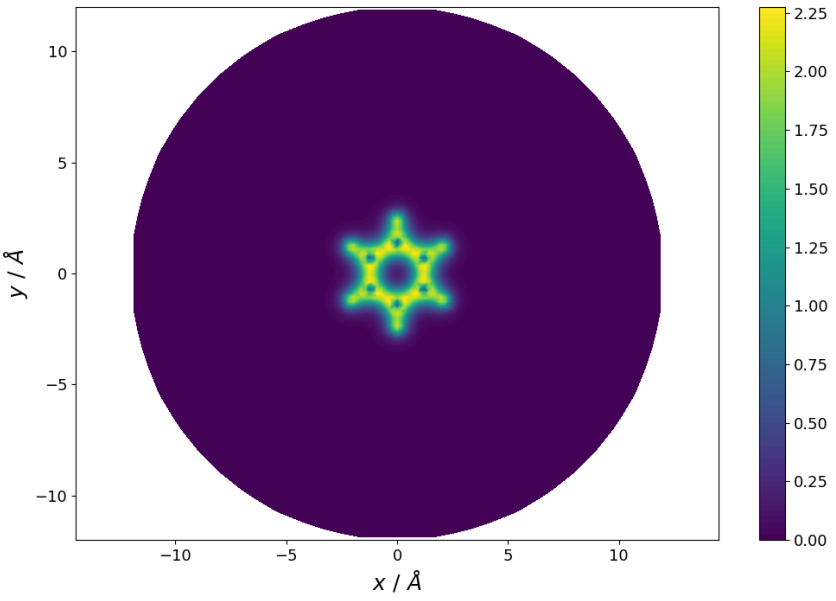

Figure 2: z=0-plane GS electron density

4.2 Finding a Sufficient AB-Width

Calculation of the *Number of Electrons*

We remind ourselves of the nature of the density:

$$n(\mathbf{r}, t) = \sum_{\sigma} \sum_{\alpha}^{occ} |\psi_{\alpha\sigma}(\mathbf{r}, t)|^2 \tag{26}$$

Since it is defined as the sum over the probability distributions - which are all normalized to one - of all occupied states, i.e. over all valence electrons (the inner electrons are included by a pseudopotential), integrating over the density gives the number of valence electrons to be still found inside the simulation box.

To do so, a discrete integration was applied: Due to the grid spacing s being the same in all directions the integration formula takes the convenient form

$$N_{\text{el}}(n;t) = \left(\sum_{\mathbf{r}} n(\mathbf{r},t) \right) * s^3 \tag{27}$$

Thus, summing the density over all grid points and multiplying it by s^3, which correspond to the cartesian infinitesimal $dxdydz$, the number of electrons, N_{el}, is received. N_{el} as defined in (27) can be seen as a density functional, as these were introduced in Section 2.2.
In the following a time-dependent evolution of N_{el} for the different AB-widths (results from the simulations in Section 3.3.1) will be plotted.

Results

The calculations were done by applying 9 different AB-widths: 0.1 Å, 0.25 Å, 0.5 Å, 0.75 Å, 1 Å, 2 Å, 3 Å, 4 Å, 5 Å.

The time-dependent number of electrons, according to (27), is plotted for the different AB-widths in Figure 3.

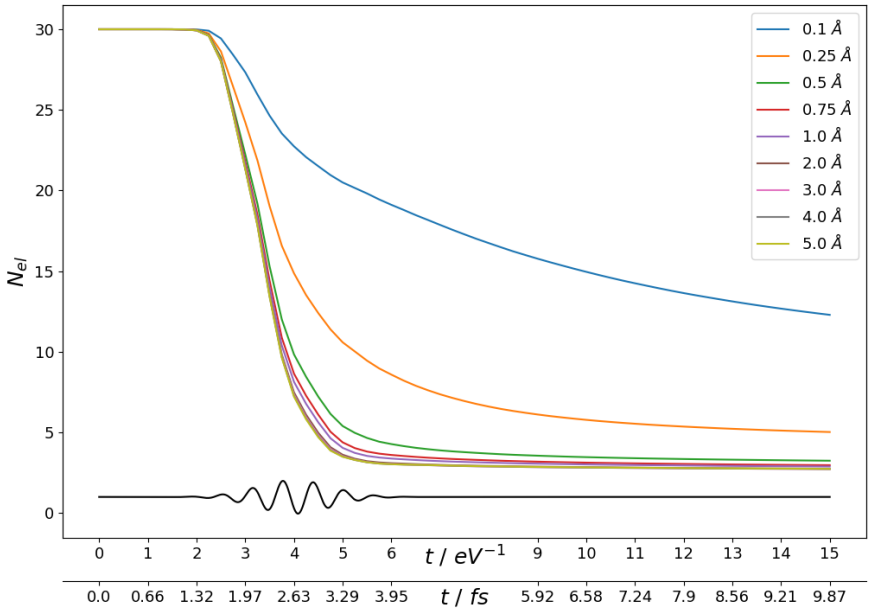

Figure 3: Time-dependent number of electrons for different AB-widths; black line: time evolution of the lasers' electric field in arb. units

We see that an AB-width of 0.5 Å – 0.75 Å is already small enough to absorb approximately the same number of photoelectrons as for larger ABs. The second part of the time-dependent calculations was done with an AB-width of 2 Å (see Section 3.3.2), because, as can be seen from Figure 3, very good agreement with larger widths is achieved.

4.3 Intensity Dependence of N_{el}

Figure 4 shows the results from the calculations in Section 3.3.2, i.e. N_{el} for different laser intensities.

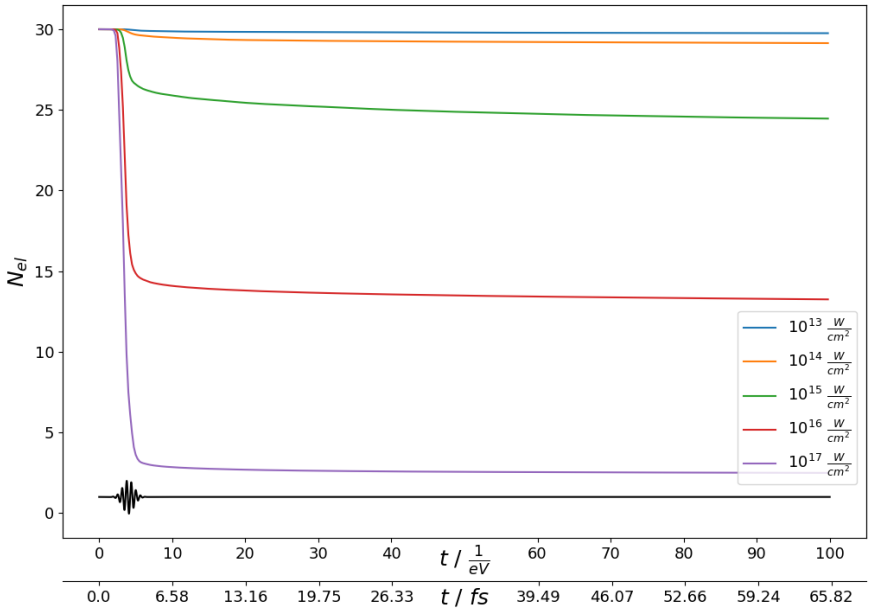

Figure 4: N_{el} for different laser intensities; black line: time evolution of the lasers' electric field in arb. units

However, as can be easily seen from the $10^{15}\ W/cm^2$ line, N_{el} does converge very slowly, possibly due to density being partially reflected from the AB (see Section 5).
In order to receive a guess for the converged values of N_{el}, a least squares fit with the model-function

$$f(t) = a_1 \times e^{-b_1 \times t - d_1} + a_2 \times e^{-b_2 \times t - d_2} + c \tag{28}$$

was performed, applying an exponential function, since, as can be seen from Figure 4, the decay of N_{el} takes an exponential form. Demanding b_1 and b_2 to be positive, *f(t)* converges towards c. Table 2 gives the time interval, the fit was performed on (i.e. the time interval where the exponential behavior of N_{el} is given), as well as c rounded to two digits for the different intensities.

Table 2: Time interval Δt and converged values c of least squares fit for different intensities I

I / $\frac{W}{cm^2}$	Δt / $\frac{1}{eV}$	c
10^{13}	[5.75, 100]	29.73
10^{14}	[7, 100]	29.01
10^{15}	[13.75, 100]	24.25
10^{16}	[14.75, 100]	12.82
10^{17}	[13.75, 100]	2.43

As can be seen from Figure 5 the model functions fit the data points very well.

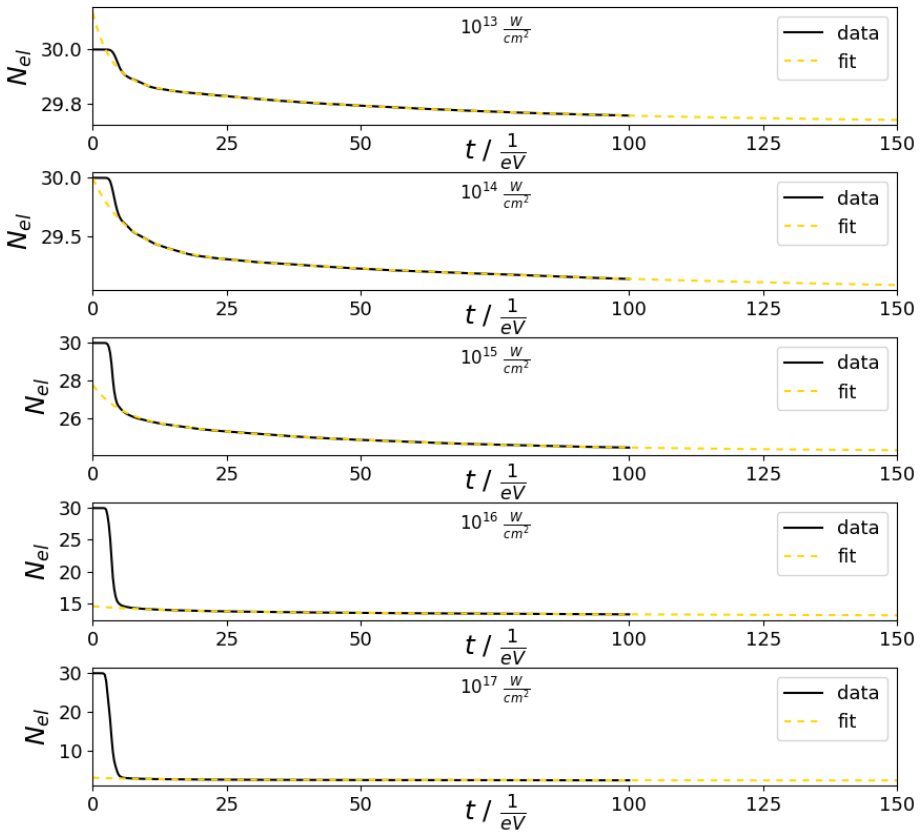

Figure 5: Exponential fit of N_{el} for different intensities

5 Discussion

The number of valence electrons remaining in the system (or more precisely: its expectation value) (c-column in Table 2) for the different intensities meet the expectation of higher intensities leading to more ionization. A major headache, however, is the very slow convergence of N_{el} (Figure 4). As the decay appears to take an exponential form, i.e. N_{el} appears to decay exponentially, a reasonable guess for this behavior is that electrons (or more precisely: electron density) get reflected from the AB (with a specific reflection coefficient), travel across the simulation box, reach the AB again, get again partially reflected, and so on (this could explain the slow decay, as well as its exponential form.). In the case of this back and forth reflections another problem may arise: The reflected density, flowing through the simulation box, could be partially bound by the (now positively-charged) benzene molecule again. Hence, it seems desireable to use ABs which minimalize these reflections. Possibly, this could be done by using a *full mask method* AB, as in [5] p.6 it is stated, that "With FMM spurious reflections are almost negligible."

6 Summary

In the present work the behaviour of benzene under strong, ultrashort laser pulses was studied, performing TDDFT calculations in the OCTOPUS-code. For a 10 eV, 1.18 fs FWHM, 10^{17} W/cm^2 laser pulse, a sufficient (mask-function) AB-width of 2 Å was found in Section 4.2. In Section 4.3 the time-dependent number of valence electrons (N_{el}) of benzene under the effect of 10 eV, 1.18 fs FWHM, 10^{13} W/cm^2 $-$ 10^{17} W/cm^2 laser pulses was studied. Performing a least squares fit the converged values of N_{el} were found to be:

Table 3: Converged values c of least squares fit for different intensities I

I / $\frac{W}{cm^2}$	c
10^{13}	29.73
10^{14}	29.01
10^{15}	24.25
10^{16}	12.82
10^{17}	2.43

References

[1] B. Engquist, A. Majda. *Absorbing Boundary Conditions for the Numerical Simulation of Waves.* Mathematics of Computation **31** (1977) 629.

[2] D. Sholl, J. Steckel. *Density Functional Theory: A Practical Introduction.* Wiley, 2009.

[3] F. Nogueira, M. A. L. Marques, C. Fiolhais. *A primer in density functional theory.* Lecture Notes in Physics. Springer, Berlin, 2003.

[4] M. A. Marques, C. A. Ullrich, F. Nogueira, A. Rubio, K. Burke, E. K. U. Gross. *Time-Dependent Density Functional Theory.* Springer, Berlin, 2006.

[5] U. De Giovannini, D. Varsano, M. A. Marques, H. Appel, E. K. Gross, A. Rubio. *Ab initio angle-and energy-resolved photoelectron spectroscopy with time-dependent density-functional theory.* Physical Review A **85** (2012) 062515.

[6] Time-Dependent. `https://octopus-code.org/doc/7.3/html/vars/Time-Dependent.html`. [Online; accessed 8-June-2019].

[7] U. De Giovannini, A. H. Larsen, A. Rubio. *Modeling electron dynamics coupled to continuum states in finite volumes with absorbing boundaries.* The European Physical Journal B **88** (2015) 56.

[8] Manual:Units. `https://octopus-code.org/wiki/Manual:Units`. [Online; accessed 31-May-2019].